JBC RESEARCH ARTICLE

The regulatory role of the *Aspergillus flavus* core retromer complex in aflatoxin metabolism

Received for publication, December 1, 2021, and in revised form, May 25, 2022 Published, Papers in Press, June 10, 2022,
https://doi.org/10.1016/j.jbc.2022.102120

Sen Wang[1,‡], Yu Wang[1,‡], Yinghang Liu[1,‡], Lin Liu[1], Jinyu Li[2], Kunlong Yang[1], Mengxin Liu[1], Wanlin Zeng[1], Ling Qin[1], Ranxun Lin[1], Xinyi Nie[1], Longguang Jiang[2], and Shihua Wang[1,*]

From the [1]State Key Laboratory of Ecological Pest Control for Fujian and Taiwan Crops, Key Laboratory of Pathogenic Fungi and Mycotoxins of Fujian Province, and School of Life Sciences, Fujian Agriculture and Forestry University, Fuzhou, Fujian, China; [2]College of Chemistry, Fuzhou University, Fuzhou, Fujian, China

Edited by Ursula Jakob

Aflatoxins are a series of highly toxic and carcinogenic secondary metabolites that are synthesized by *Aspergillus* species. The degradation of aflatoxin enzymes is an important regulatory mechanism which modulates mycotoxin producing. The retromer complex is responsible for the retrograde transport of specific biomolecules and the vacuolar fusion in the intracellular transport. Late endosomal-associated GTPase (Rab7) has been shown to be a downstream effector protein of the retromer complex. A deficiency in the retromer complex or Rab7 results in several cellular trafficking problems in yeast and humans, like protein abnormal accumulation. However, whether retromer dysfunction is involved in aflatoxin synthesis remains unclear. Here, we report that the core retromer complex, which comprises three vacuolar protein sorting-associated proteins (AflVps26-AflVps29-AflVps35), is essential for the development of dormant and resistant fungal forms such as conidia (asexual reproductive spore) and sclerotia (hardened fungal mycelium), as well as aflatoxin production and pathogenicity, in *Aspergillus flavus*. In particular, we show the AflVps26-AflVps29-AflVps35 complex is negatively correlated with aflatoxin exportation. Structural simulation, site-specific mutagenesis, and coimmunoprecipitation experiments showed that interactions among AflVps26, AflVps29, and AflVps35 played crucial roles in the retromer complex executing its core functions. We further found an intrinsic connection between AflRab7 and the retromer involved in vesicle-vacuole fusion, which in turn affected the accumulation of aflatoxin synthesis-associated enzymes, suggesting that they work together to regulate the production of toxins. Overall, these results provide mechanistic insights that contribute to our understanding of the regulatory role of the core retromer complex in aflatoxin metabolism.

Aspergillus flavus, an important species of saprophytic and toxigenic fungus (1), is commonly found in soil, dust, air, spoiled crops, and food and has a serious impact on preharvest and postharvest seed crops due to its pathogenicity (2, 3). As an opportunistic fungus, *A. flavus* causes aspergillosis diseases in immunologically deficient animals and humans (4). Furthermore, aflatoxins that are synthesized by several species of *Aspergilli* exhibit strong toxicity and carcinogenic effects in humans. The long-term ingestion of low doses of these secondary metabolites triggers poisoning symptoms (e.g., immune system damage) and increases cancer risk (5–7).

To date, several aflatoxins and derivatives have been discovered in *A. flavus*, including aflatoxin B1 (AFB1) (8). AFB1 has attracted much attention, as the long-term exposure to this toxin increases the chances of developing cancer in humans. The synthesis of AFB1 is a complex process involving various enzyme-catalyzed reactions (9–13) (Fig. S1), and the corresponding intermediates in the biosynthesis pathway are produced in specific organelles (12, 13) (Fig. S1). In previous studies, highly expressed Nor-1 (AflD) in the cytoplasm was found to convert norsolorinic acid to avilantine at the early stages of AFB1 synthesis (12, 14–17). Ver-1 (AflM), which is also localized in the cytoplasm, catalyzes versicolorin A into demethylated staphylococcal toxin during the middle periods of enzyme reactions (17–19). OmtA (AflP) plays a methyltransferase role in synthesizing O-methylsterigmatocystin from sterigmatocystin during the final steps of AFB1 production. Interestingly, the subcellular location of AflP is in the vesicles, which is quite different from AflD or AlfM (17, 20).

The retromer is a multiprotein complex that functions at the endosomes to regulate the recognition of specific biomolecules and to mediate the retrieval of these cargo molecules from the endocytic system back to the trans-Golgi network trafficking system (21–23). The retromer complex is divided into two distinct subcomplexes in yeast: one is a dimer subunit composed of two vacuolar protein sorting-associated proteins (Vps5 and Vps17), which participates in the recognition of endosomal membrane bending and contributes to the formation of tubules or vesicles on membranes (23, 24). The other subcomplex is known as the core retromer, which is composed of three proteins (Vps26, Vps29, and Vps35) that have been identified in the transportation of cargo molecules and the control of the cellular localization of these shipments (23, 24). In previous studies, the Vps26–Vps29–Vps35 subcomplex was placed like an

‡ These authors contributed equally to this work.
* For correspondence: Shihua Wang, wshyyl@sina.com.

arched bridge on the surface of membranes (25, 26). Vps35 is arranged as a 'leg' of the arch and supports the apex building (Vps29), while Vps29 is exposed to the cytoplasm, suggesting that this part of the subcomplex could facilitate the recruitment of cytosolic regulatory factors (27, 28). In addition, Vps26 from the pier of arches is connected to the N-terminal of Vps35. The Vps26–Vps29–Vps35 subcomplex performs biological functions effectively as a whole. In *Saccharomyces cerevisiae,* this protein complex is required for the localization and stability of Vps10 (29). The disruption of the coding genes of Vps26, Vps29, or Vps35 obviously affects growth, development, and pathogenicity in *Fusarium graminearum* (30). The ternary-protein complex participates in the regulation of autophagosome formation in *Magnaporthe grisea*, and Vps35 is believed to interact with the autophagy-related protein (Atg8) directly and to modulate its recycling from the vacuole to autophagosome (31). In addition, the protein storage vacuoles of the Vps35 mutant are smaller than that of the WT in *Arabidopsis* (32).

Ras-associated binding GTPases (Rab), also named Ypt (yeast protein transport), cycle between GTP-bound (active) and GDP-bound (inactive) states and play a role as molecular switches in the regulation of membrane trafficking in eukaryotes (33). Two small GTPases, Rab5 and Rab7, have been shown to recruit retromers during early endosome and late endosome formation, respectively (34, 35). These 'late' endosomes are further fused with vacuoles/lysosomes so that their cargo molecules can be digested by the vacuolar/lysosomal hydrolases pathway. The absence of Rab7 will result in the formation of minivacuoles due to the endosome not having undergone the late fusion stage (36, 37). In addition, Rab7 specifically interacts with the carboxy terminus of Vps26 of the cargo-selective trimer in a vesicular transportation manner (38). Rab7 then binds with the N-terminal regions of Vps35 directly, and the binding affinity of Rab7-Vps35 is enhanced in the presence of Vps26 (39). In *Arabidopsis*, Rabg3f (the Rab7 homologous family) is necessary for endosomal circulation and directly binds to Vps35 (34). First, Vps35–Rabg3f interaction is necessary for the complex assembly of HOPS and the fusion of late vacuoles as a checkpoint in the control of traffic toward the vacuole (40). Vps41 (HOPS complex subunit)-Rab7 then mediates the fusion of late endosomes/vacuoles (41).

In this study, we report that the core retromer complex plays a vital role in regulating growth, development, pathogenicity, and aflatoxin synthesis in *A. flavus*. The deletion of any subunit of the retromer subcomplex, such as AflVps35, AflVps26, or AflVps29, could lead to a similar defective phenotype, particularly regarding toxin production. By using structural simulation, site-specific mutations, and coimmunoprecipitation (CoIP) experiments, we demonstrated that interactions among these three proteins are necessary for the retromer to execute its core functions. In addition, AflVps35 bound to AflRab7, together regulating vacuole formation and thereby affecting the synthesis of aflatoxins. Therefore, these results may improve our understanding of the regulatory mechanism of the core retromer complex in fungal toxin metabolism.

Results

AflVps35 is important for conidia development, sclerotia formation, and pathogenicity in A. flavus

In order to clarify the role of AflVps35 in *A. flavus*, an Δ*Aflvps35* mutant was constructed with homologous recombination using *Aspergillus fumigatus pyrG* as the screening gene and the CA14 strain as the background strain. Verified by PCR, real-time PCR, and southern blot procedures (Fig. S2, *A–D*), the Δ*Aflvps35* deletion mutant was then used for generating the complementation strain (Com-*Aflvps35*) (Fig. S2, *A* and *B*). Based on microscopic inspection and statistical analysis, the colony diameter of the deletion strain had been reduced to less half than those of the WT and complementation strains (Fig. 1, *A* and *B*). The mycelium in Δ*Aflvps35* had shrunk in size and formed more branches, and the fungal colony exhibited denser phenotypic characteristics (Fig. S3*A*).

Dissemination of spores in the environment is an important propagation method for *A. flavus.* It was observed that the Δ*Aflvps35* strain was unable to form a conidial stalk, while WT and Com-*Aflv*ps35 exhibited normal development in this region (Fig. 1*C*). The abnormal phenotype change in the deletion strain was also reflected in the statistical analysis of the spore number, in that there was no significant difference in the amount of conidia between Com-*Aflvps35* and WT, except those of Δ*Aflvps35* (Fig. 1*D*). The transcription levels of the two key genes (*abaA* and *brlA*) involved in spore formation were drastically reduced in the Δ*Aflvps35* strain compared with the other strains (Fig. S4*K*). The formation of sclerotia in *A. flavus* is an indicator of reproduction. The sclerotial generation was abolished in the dysfunctional *Aflvps35* strain (Fig. 1, *E* and *F*), while that of the WT and Com-*Aflvps35* developed normally. Moreover, the expression level of the sclerotia-related genes (*nsdC* and *nsdD*) in the Δ*Aflvps35* strain was far lower than that in the WT and Com-*Aflvps35* strain (Fig. S4*L*).

Pathogenicity is a critical feature of *A. flavus,* causing a decline in the quality of agricultural products. In the infection assay, the Δ*Aflvps35* strain colonized part of the surface of peanuts, with neither conidia nor hyphae sporulating on the maize seed coat, indicating that the virulence level of the disruptive strain had receded and even lost completely compared with the other two strains (Fig. S8, *A* and *B*). The low pathogenicity of the deletion strain was also reflected in the significantly decreased spore number in the infected seeds (Fig. S8, *C* and *D*). Furthermore, the resistance of the Δ*Aflvps35* strain to oxidants, cell membrane, and cell wall inhibitors was also reduced (Fig. S3, *B–E*). All the aforementioned results suggested that AflVps35 is important in the regulation of conidia development, sclerotia formation, and pathogenicity in *A. flavus.*

The regulatory effects of AflVps35 are negatively correlated with aflatoxin production/exportation and the accumulation of aflatoxin synthesis-associated enzymes but not relevant to aflatoxin synthesis-related gene expression

Three *A. flavus* strains (WT, Δ*Aflvps35*, and Com-*Aflvps35*) were cultured for aflatoxin extraction and analysis. By using

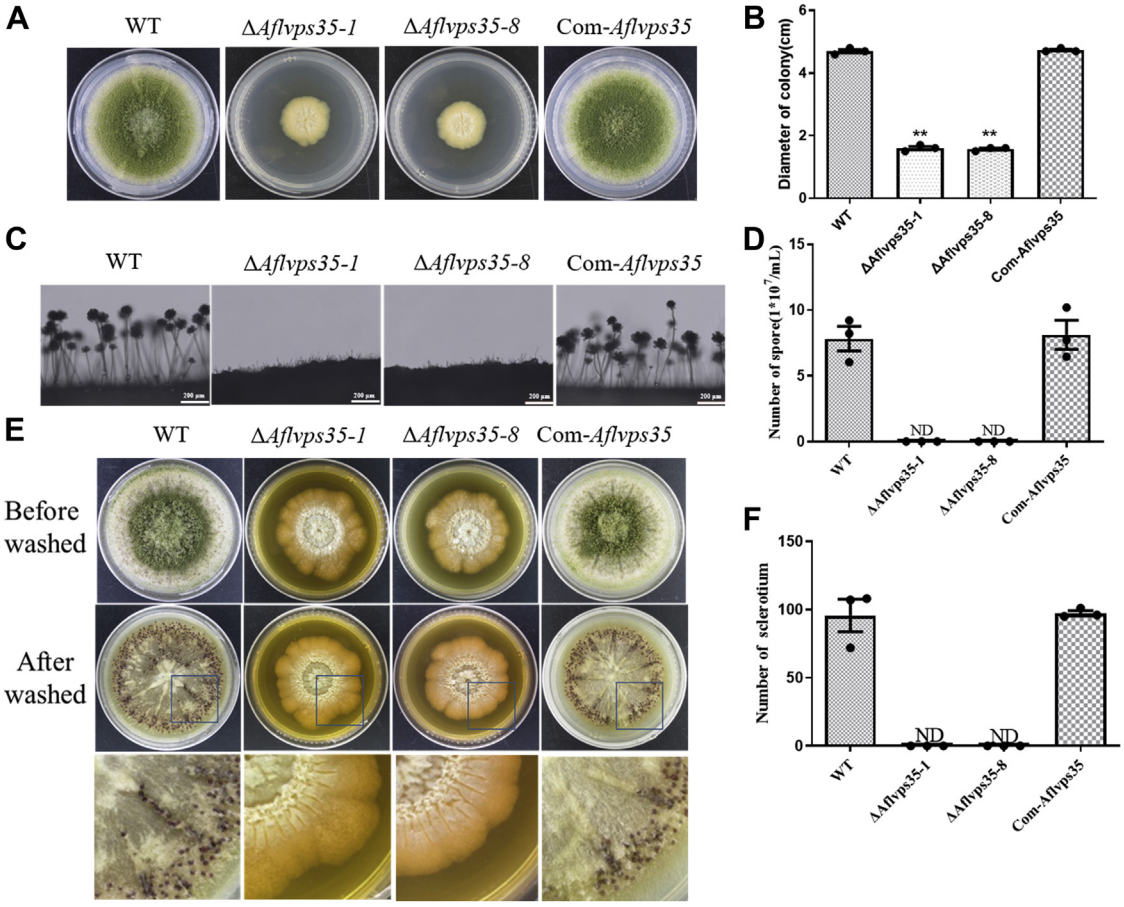

Figure 1. AflVps35 regulates conidia and sclerotia formation in *Aspergillus* flavus. *A*, the colony morphology of WT, Δ*Aflvps35*, and Com-*Aflvps35* strains on PDA medium. *B*, statistical analysis of the diameter as panel A. *C*, microscopic view of the conidiophore formation of the WT, Δ*Aflvps35*, and Com-*Aflvps35* strains. *D*, amounts of conidia produced by the above three *A. flavus* strains on PDA medium. *E*, phenotypic observation of sclerotia formation in different *A. flavus* strains on WKM medium. *F*, number of sclerotia produced by the indicated *A. flavus* strains (panel E). ** indicates a significance level of $p < 0.01$ based on one-way ANOVA with three replicates. All experiments described above had three biological replicates. PDA, potato dextrose agar; WKM, Wickerham.

TLC detection and optical density analysis, we found that the AFB1 released from Δ*Aflvps35* in the medium was increased by more than twice than those from the WT and complemented strains (Fig. 2, *A* and *B*). Using HPLC, the AFB1 secretion levels of the three strains were found to be consistent with the TLC detection results (Fig. 2*C*). We found that a similar phenomenon existed in the toxin extracted from the seeds colonized by the Δ*Aflvps35* strain (Fig. 2, *I–L*). In addition, the amount of AFB1 as residue was noticeably different between the peanut and maize kernels infected by the Δ*Aflvps35* strain. This discrepancy is most likely due to differences in species resistance between peanuts and maize seeds, and the deletion strain could not easily colonize the surface of the maize seeds.

Interestingly, there was no change in the transcription level of the aflatoxin-related genes *aflD*, *aflM*, and *aflP* (Fig. 2*D*). We extracted toxins from the vesicles of *A. flavus* and found that the loss of the *Aflvps35* gene induced a sharp increase in the amount of toxins in the vesicles as well (Fig. 2, *E* and *F*). We focused on whether biosynthesis-encoding genes in different aflatoxin synthesis stages could control metabolite production in the Δ*Aflvps35* strain. Intriguingly, the protein expression levels of early (AflD), middle (AflM), and late (AflP) aflatoxin enzymes increased at least 1.5-fold in the KO strain, as determined by densitometry (Fig. 2, *G* and *H*), while the mRNA levels of these encoding genes in Δ*Aflvps35* were consistent with that in the WT and complemented strains (Fig. 2*D*). Therefore, it was concluded that there was no relation between the increase in aflatoxin output in the medium and the transcription of aflatoxin biosynthesis-encoding genes in Δ*Aflvps35*. The cause of the constantly upregulated toxin may be that aflatoxin synthesis-associated enzymes were more easily accumulated in the deletion strain.

AflVps35 forms a functional complex with AflVps26 and AflVps29 locating on the vacuole

As previously described, Vps35, Vps26, and Vps29 form a trimer subunit for selective cargo loading in yeast, plants, and mammals (23, 24). Firstly, an AflVps35-GFP strain bearing a GFP marker was generated to identify the subcellular location of the target protein in *A. flavus*. Under fluorescence microscope observation, AflVps35-GFP was expressed on the surface of hyphal vacuoles that is consistent with the staining location by vacuole lumen dye (CMAC) and vacuole membrane stain (FM4-64) (Fig. 3, *A* and *B*). As expected, AflVps26

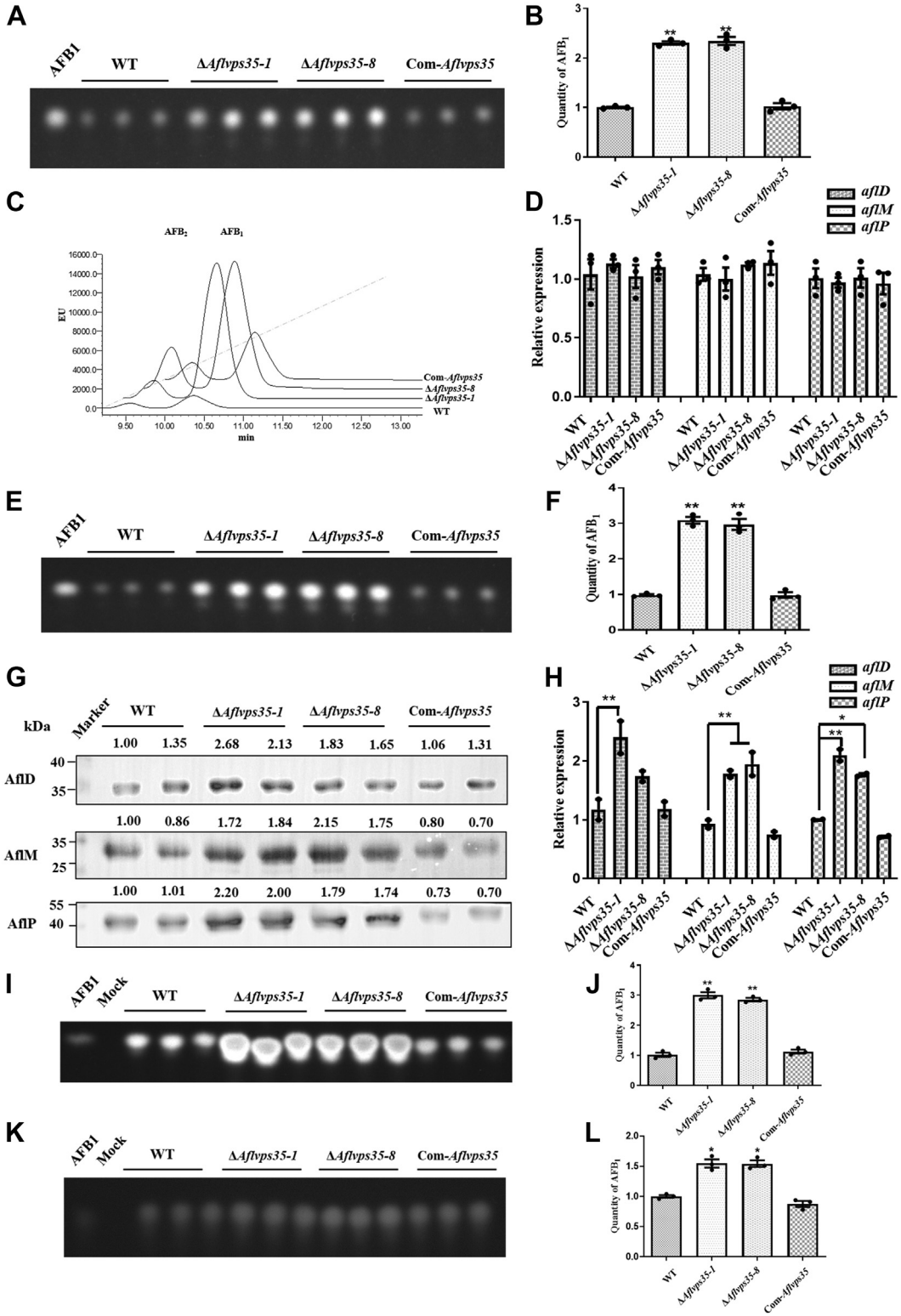

Figure 2. Effects of *Aflvps35* on AFB1 production in *Aspergillus flavus*. *A*, TLC analysis of AFB1 production in *A. flavus* WT, Δ*Aflvps35*, and Com-*Aflvps35* strains with three biological replicates. *B*, optical density analysis of AFB1 production (panel A). *C*, HPLC analysis of AFB1 production in different strains. *D*, relative expression of the *aflD*, *aflM*, and *aflP* genes in the three above strains with three biological replicates. *E*, TLC analysis of AFB1 in the vesicles of different strains with three biological replicates. *F*, optical density analysis of AFB1 in the vesicles (panel E). *G*, accumulation of aflatoxin synthesis–related enzymes in the early (AflD), middle (AflM), and late stage (AflP) with two biological replicates. Quantitative analysis of loaded total protein for the Western blot is shown in Fig. S5*A*. *H*, optical density analysis of the accumulation of aflatoxin synthesis–related enzymes (panel G). *I*, TLC analysis of AFB1 production in different strains during peanut infection with three biological replicates. *J*, optical density analysis of AFB1 production (panel I). *K*, TLC analysis of AFB1 production in different strains during maize infection with three biological replicates. *L*, optical density analysis of AFB1 production during maize infection (panel K). * indicates a significance level of $p < 0.05$, ** indicates a significance level of $p < 0.01$ based on one-way ANOVA with three biological replicates. AFB1, aflatoxin B1.

and AflVsp29 shared the same positions with AflVps35, surrounding the membrane of the vacuole (Fig. S7, *C* and *F*).

Two mutant strains (HA-AflVps26 and HA-AflVps35) were then generated for CoIP validation. The anti-HA antibody pulled down both AflVps26 and AflVps35 in the cell extracts of the HA-AflVps26 strain (see lane IP) (Fig. 3*C*), and immunoprecipitation with the same antibody from the HA-AflVps35 strain lysate indicated that AflVps29 physically bound to AflVps35 (Fig. 3*D*). These results reflect the linkage among AflVps35, AflVps29, and AflVps26 as a protein complex *in vivo*.

We finally investigated the biological function of AflVps26 and AflVps29 in *A. flavus*. *Aflvps29* and *Aflvps26* KO and complementation experiments were carried out, and the genetic engineering strains were identified by PCR and Southern blot analysis (Fig. S2, *A–D*). Compared to the WT and complementation strains, the defects of the Δ*Aflvps26* and Δ*Aflvps29* mutants appeared on the conidia, sclerotia formation, response to environmental stresses and pathogenicity, which is similar to the Δ*Aflvps35* mutant (Figs. 4, S3, *B–E*, S4, *A–J*, and S8). Surprisingly, the Δ*Aflvps26* and Δ*Aflvps29* mutants secreted significantly higher levels of aflatoxin, as

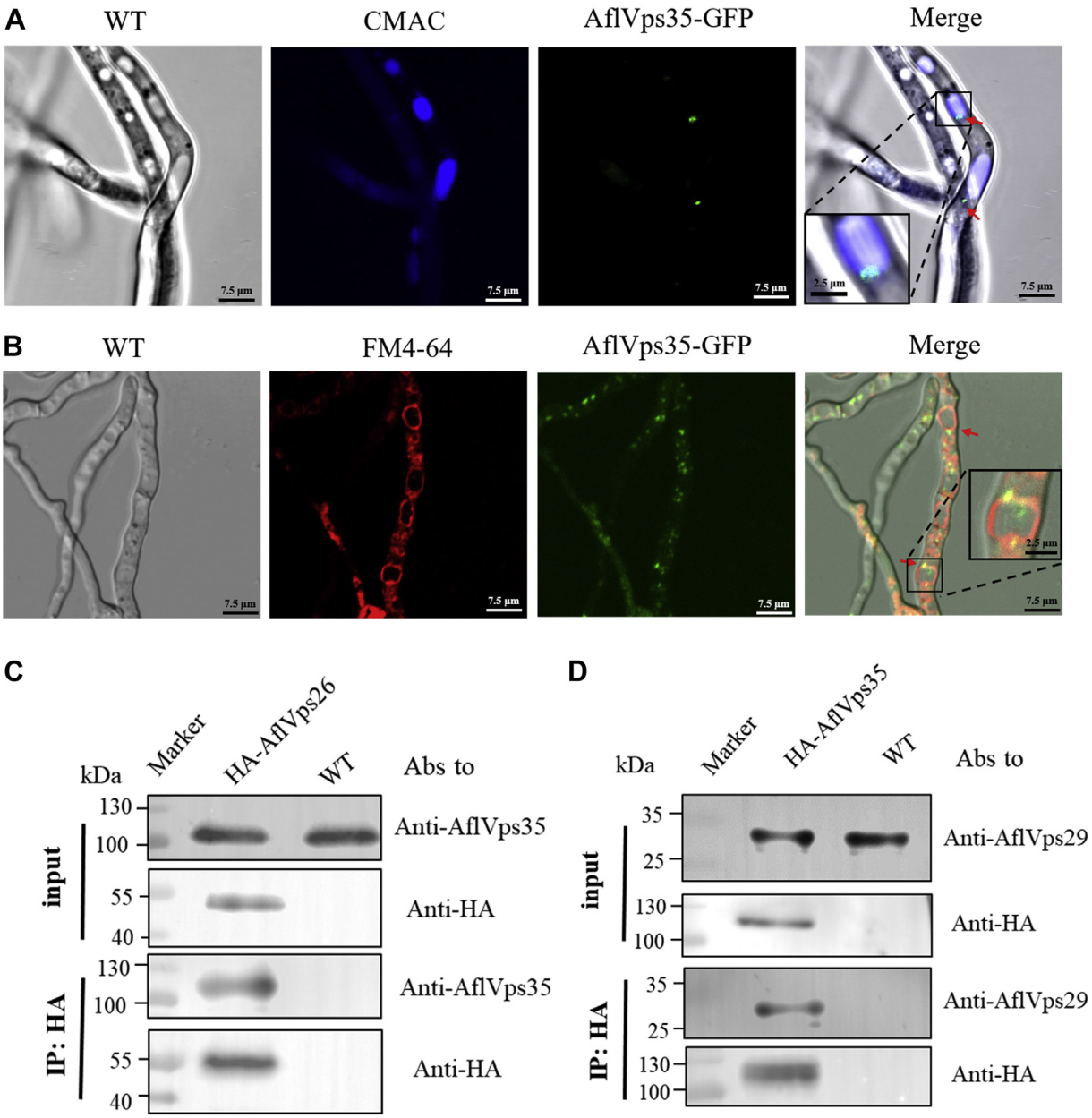

Figure 3. AflVps35 is localized on the vacuole surface and interacts with AflVps26 and AflVps29 proteins in *Aspergillus flavus*. *A*, the subcellular distribution of the AflVps35-GFP fusion protein in *A. flavus*. The vacuolar dye CMAC was used to stain the vacuoles. *B*, FM4-64 was used to stain the vacuoles, and the subcellular localization of Vps35-GFP in *A. flavus* was observed. *C*, lysates from *A. flavus* WT or HA-tagged AflVps26 were subjected to immunoprecipitation (IP) using an anti-HA tag antibody. Lysates (*bottom*) and immunoprecipitates (*top*) were detected by Western blot with antibodies (Abs) against the HA tag and AflVps35-N, respectively. *D*, the CoIP analysis suggests an interplay between AflVps29 and AflVps35. CoIP, coimmunoprecipitation.

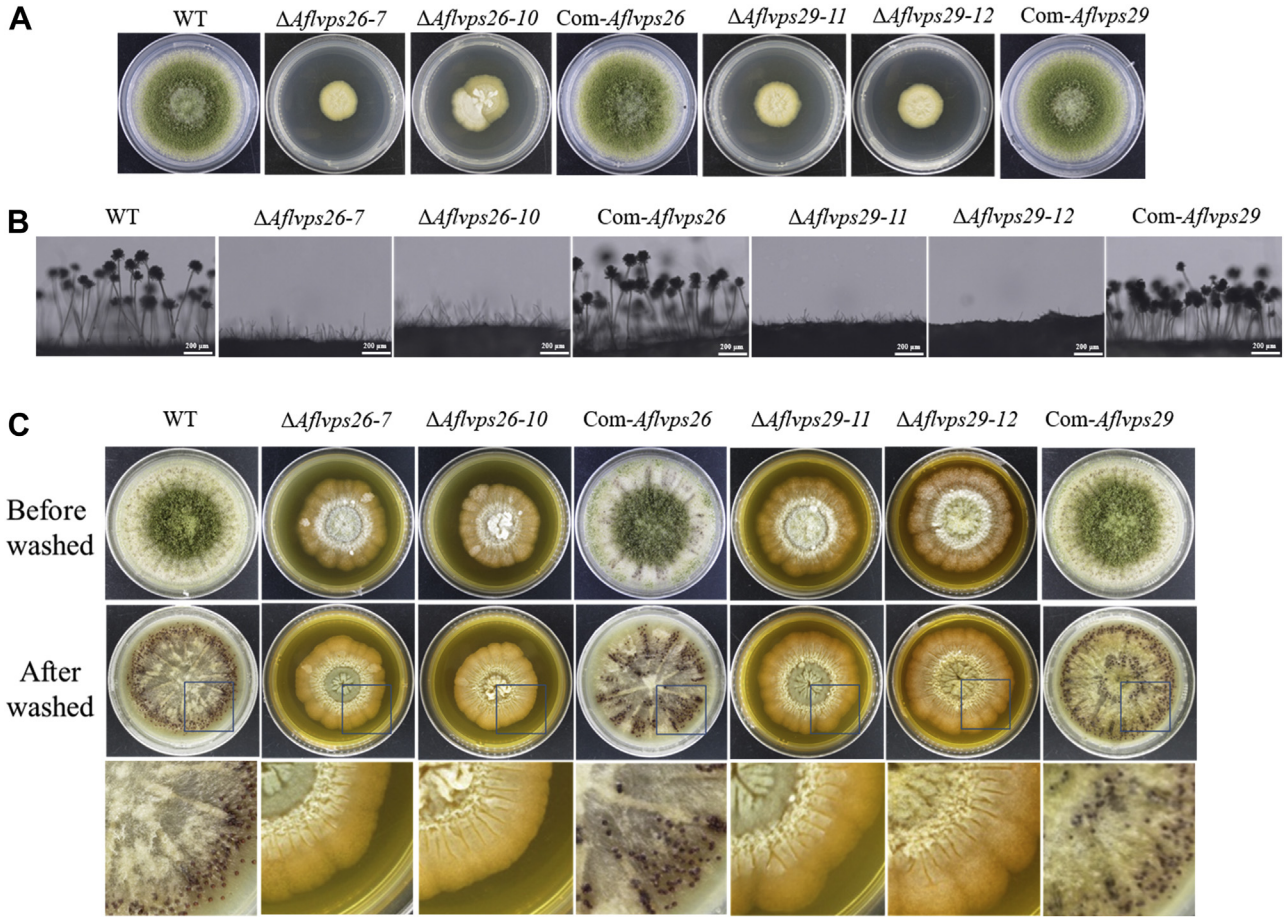

Figure 4. Effects of *Aflvps26* and *Aflvps29* on fungal growth and development in *Aspergillus flavus*. *A*, the colony morphology of WT, Δ*Aflvps26*, Com-*Aflvps26*, Δ*Aflvps29*, and Com-*Aflvps29* on PDA medium. *B*, microscopic view of the conidia of WT, Δ*Aflvps26*, Com-*Aflvps26*, Δ*Aflvps29*, and Com-*Aflvps29* strains on PDA medium. *C*, phenotypic observation of the sclerotia of WT, Δ*Aflvps26*, Com-*Aflvps26*, Δ*Aflvps29*, and Com-*Aflvps29* on WKM medium. All experiments described above had three biological replicates. PDA, potato dextrose agar; WKM, Wickerham.

Δ*Aflvps35* did in liquid culture and the seed infection process (Figs. S6, S7, *A*, *B*, *D* and *E*, S8, *I*–*L*).

Molecular dynamics and molecular docking revealed the key residues of the retromer subcomplex

To further illuminate the binding features, we performed all-atomic molecular dynamics (MD) simulations on the retromer complex. Given that the binding sites of AflVps26 and AflVps29 upon AflVps35 were reasonably distant, we performed two individual MD simulations: one of molecular dockings between AflVps26 and the N-terminal region of AflVps35 (13–307), and the other between AflVps29 and the C-terminal region of AflVps35 (565–867). During the simulation process, two complexes, referred to as AflVps26-AflVps35N and AflVps29-AflVps35C, remained intact and did not disassociate. RMSD analysis suggested that the protein conformations for each complex did not obviously change through the evolution occurring during the MD procedure (Fig. S9*N*).

For complex AflVps26–AflVps35, AflVps26 merely attached itself to the N-terminal region of AflVps35. The interface area in AflVps26-AflVps35N was calculated at 527 Å^2. There were four pairs of salt bridge interactions across the interface, namely D234-R144, E241-R137, E241-K188, and R246-D131 (Fig. 5*A*). It was evident that the electrostatic attractions played a key role in securing AflVps26–AflVps35N interactions. Additionally, E231 from AflVps26 could stably establish hydrogen bonds with N102 and I103 from AflVps35 (Fig. 5*A*). In the AflVps29–AflVps35C complex structure, AflVps29 was partially surrounded by the C-terminal region of AflVps35. The interface area in AflVps29-AflVps35C was estimated at 924 Å^2. The number of salt bridge interactions increased as the binding interface expanded. Both D111 and E153 from AflVps29 developed two salt bridge interactions with arginine residues from AflVps35 (D111-R855, D111-R859, E153-R619, E153-R622) (Fig. 5*B*). Additionally, MD simulation suggested the presence of the salt bridges D16-R607 and E129-R865. Hydrogen bonds were also common across the interface. For example, Q570 and R666 from AflVps35 are connected to the backbone oxygen atoms of AflVps29 via such noncovalent interactions. Other hydrogen bonds regularly observed *in silico* were, to name a few, S70-Q707, D99-Y814, R108-N810, and Y147-D676. Notably, Q707 from AflVps35 is not conserved in mammals and plants, indicating that the S70–Q707 interaction is characteristic of *A. flavus* (Fig. 5*B*).

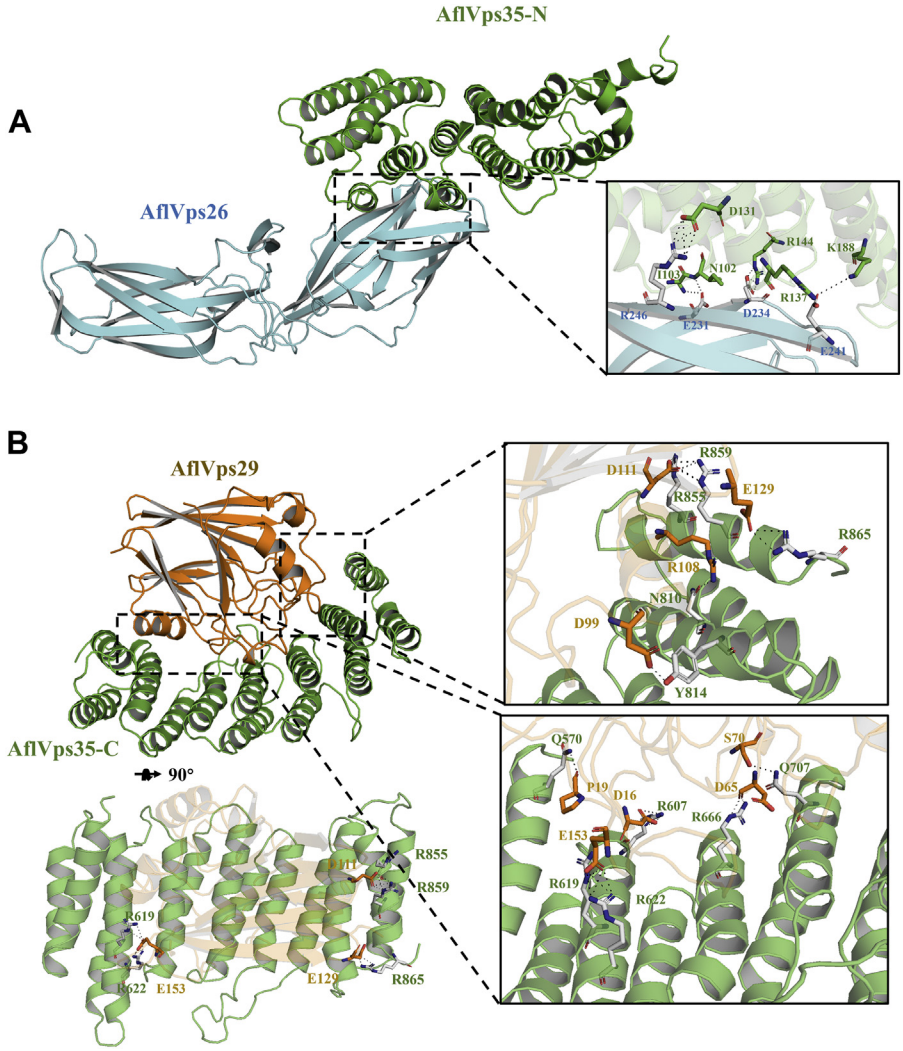

Figure 5. Overall structure of the core retromer complex (AflVps35, AflVps26, and AflVps29) of the retromer. The overall structure of the core retromer complex is shown as a *cartoon* and is colored by different subunits (Vps26 in *blue*, Vps29 in *yellow*, and Vps35 in *green*). *A*, hydrogen-bond interactions between AflVps35 and AflVps26. *B*, Hydrogen bonds or salt bridges between AflVps35 and AflVps29.

Breaking interactions among the AflVps26–AflVps29–AflVps35 complex induced aflatoxin synthesis/export increases

To obtain structural information of the MD, a series of HA-tagged AflVps26 or AflVps35 mutants was prepared (Fig. S9, *A–M*) to verify whether the prediction residues were important for Vps protein interactions. In the cross-linking of AflVps35 to AflVps26 mutant proteins (Fig. 6*A*), the protein–protein recognition capability in all mutants was weaker than in the WT strain in terms of lost salt or hydrogen bridges. The morphological characteristics of these four AflVps26 mutants ($AflVps26^{E231A}$, $AflVps26^{D234A}$, $AflVps26^{E241A}$, and $AflVps26^{R246A}$) were similar to those observed in the mutant strains lacking AflVps26 and AflVps35, as reflected in the decreased colony diameter (Fig. 6, *C* and *D*). Consistent with the AflVps26 or AflVps35 deletion strains, there was no significant change in the transcription levels of aflatoxin synthesis-related genes with an increase in the toxin (Fig. S10, *A–C*). In another group of CoIP experiments, we also found that the binding ability of the AflVps35 to AflVps29 mutant proteins became weaker (Fig. 6*B*). The combination was completely abolished when both salt bridges (in $AflVps35^{R619A\ R622A\ R855A\ R859A\ R865A}$ strain) were destroyed (Fig. 6*B*). The phenotypic changes in the AflVps35 point mutants were similar to those in the AflVps29 or AflVps35 deletion strains, particularly regarding the high level of toxin (Figs 6, *E* and *F* and S10, *D–F*). All these results suggested that breaking the linkage on AflVps35-AflVps26 or AflVps35-AflVps29 induced aflatoxin synthesis/export increases.

AflRab7 binds to AflVps35 and regulates the synthesis of toxins

We were interested to know how aflatoxin synthesis/export is promoted in the *vps* deletion strains or mutant strains. We speculated that a potential mechanism is that a cargo-selective trimer and partners coordinately control the emissions of secondary metabolites. In previous reports, a Vps35 partner Ypt7 was necessary for vesicle-vacuole fusion and aflatoxin increase in *Aspergillus nidulans* (20). In *Arabidopsis*, the

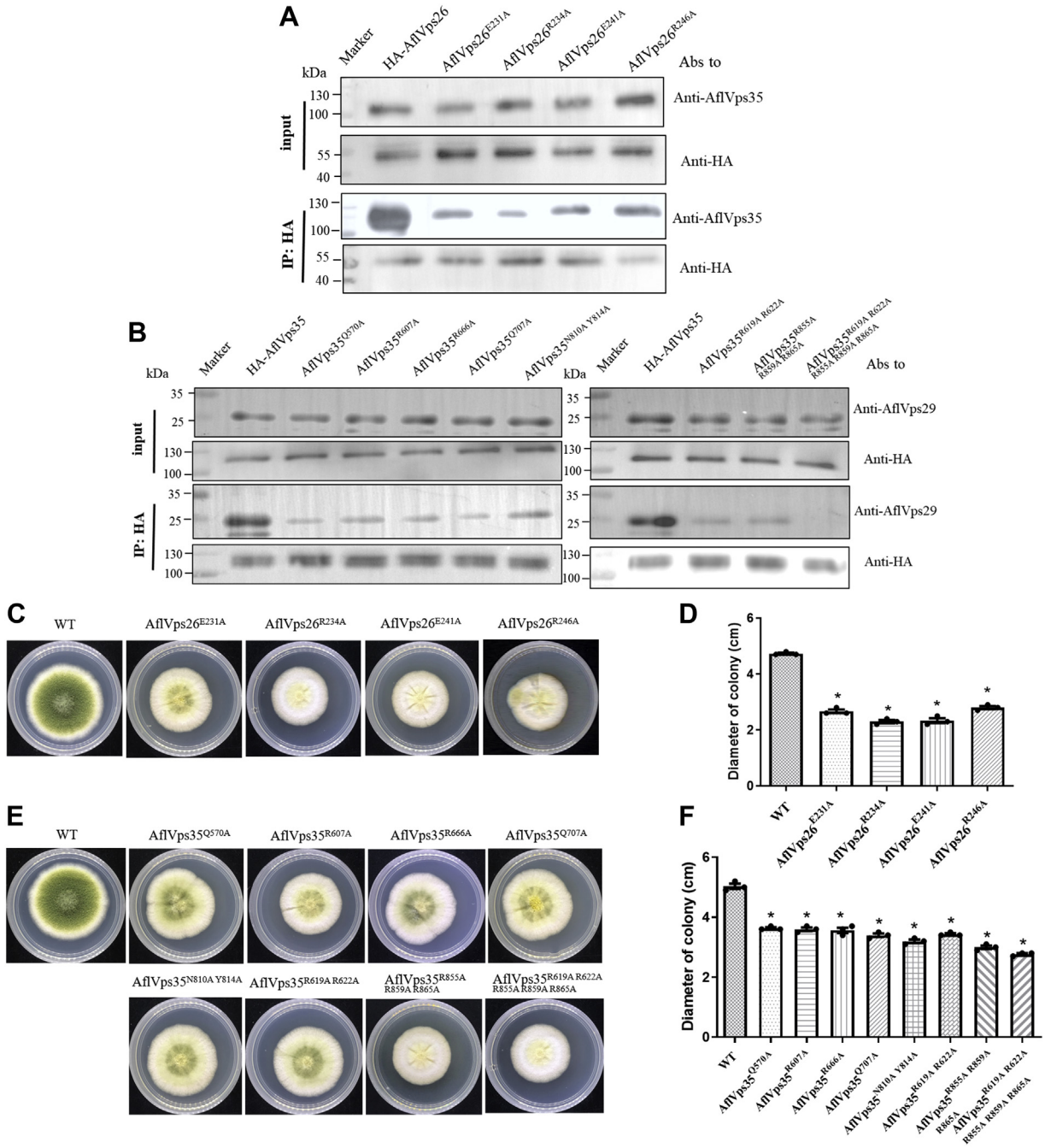

Figure 6. Identification of protein–protein interaction sites in the core retromer complex and colony growth of different AflVps26 or AflVps35 point mutants in *Aspergillus flavus*. *A*, mutations in the AflVps35-AflVps26 interacting amino acid of AflVps26 abrogate assembly. Extracts from AflVps26-HA or HA-tagged AflVps26 mutant strains were subjected to immunoprecipitation (IP) using an anti-HA tag antibody. Lysates (*bottom*) and immunoprecipitates (*top*) were evaluated by Western blot with antibodies (Abs) against the HA tag and AflVps35-N, respectively. *B*, extracts from *A. flavus* mutant Vps35-HA were subjected to IP using the anti-HA tag antibody. The Western blot analysis showed that mutations in the protein–protein interacting surface of Vps35 abrogate assembly. *C*, the colony morphology of WT and AflVps26 mutation strains on PDA medium with three biological replicates. *D*, statistical analysis of the diameter (panel C). *E*, the colony morphology of WT and AflVps35 mutation strains on PDA medium with three biological replicates. *F*, statistical analysis of the diameter (panel E). * indicates a significance level of $p < 0.05$ based on one-way ANOVA with three biological replicates. PDA, potato dextrose agar.

interaction of Vps35 homolog of Rab7 was necessary for triggering the fusion of vacuoles (40). We found that knocking-out the *Aflvps35* gene in *A. flavus* also led to the fragmentation of the vacuoles (Fig. 7*A*). Therefore, the *Ypt7* homologous gene *Aflrab7* was deleted, as confirmed by PCR (Fig. S2*A*) and Southern blot (Fig. S2*D*) in this study, and then, the CoIP method was used to determine the AflVps35–AflRab7 interaction (Fig. 7*B*). In the Δ*Aflrab7* mutant strain, the amount of aflatoxin secreted out of the cells or preserved inside the vesicles kept growing sustainably (Fig. 7, *C* and *D*) and was accompanied by the protein component (AflP) accumulating in the intracellular space (Fig. 7, *F* and *G*). However, the

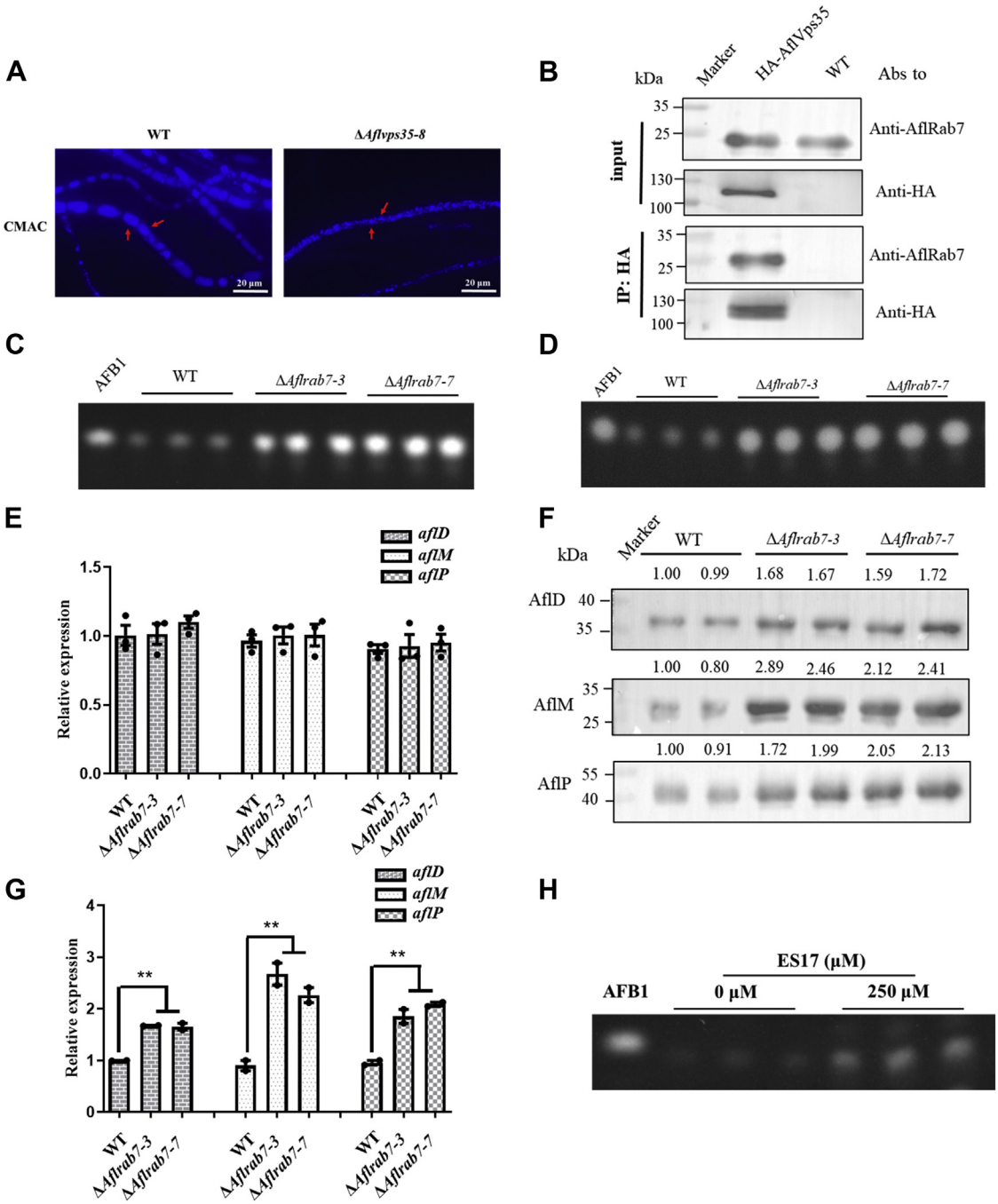

Figure 7. AflRab7 binds to AflVps35 directly and regulates aflatoxin synthesis. *A*, observation of vacuoles under the microscope with three biological replicates. *B*, lysates from *Aspergillus flavus* WT or HA-tagged AflVps35 were subjected to immunoprecipitation (IP) using a murine monoclonal antibody to the HA epitope. Lysates (*bottom*) and immunoprecipitants (*top*) were analyzed by SDS-PAGE and immunoblotted with antibodies (Abs) against the HA tag and AflVps35-N, respectively. *C*, TLC analysis of AFB1 production in *A. flavus* WT and Δ*Aflrab7* strains with three biological replicates. *D*, TLC analysis of AFB1 in the vesicles of different strains with three biological replicates. *E*, relative transcriptional level of the *aflD*, *aflM*, and *aflP* genes in different strains with three biological replicates. *F*, accumulation of aflatoxin enzyme in the early (AflD), middle (AflM), and late stage (AflP) for WT and Δ*Aflrab7* strains. Quantitative analysis of the loaded total protein for the Western blot is shown in Fig. S5*D*. *G*, optical density analysis of the accumulation of aflatoxin synthesis–related enzymes (panel F). *H*, TLC analysis of AFB1 production in *A. flavus* when a WT strain was treated with ES17 (250 μM) and control (DMSO) with three biological replicates. ** indicates a significance level of $p < 0.01$ based on one-way ANOVA with three biological replicates. AFB1, aflatoxin B1.

mRNA level of the aflatoxin-producing genes remained virtually unchanged (Fig. 7*E*). In previous studies, a small molecule compound (ES17) effectively blocked the interaction between Vps35 and Rab7 and prevented the late fusion of vacuoles in *Arabidopsis* (40). In this study, ES17 at a high concentration (above 250 μM) promoted the level of aflatoxin and inhibited the growth of fungal colonies (Figs. 7*H* and S11, *A*–*C*). This effect of ES17 in *A. flavus* was similar to the deletion of AflVps35 or AflRab7. In addition, ubiquitinated proteins in autophagosomes of *Arabidopsis* accumulated

under ES17 treatment (40). Therefore, we examined the ubiquitination levels in WT and *Aflvps35* deletion mutants and found that the level of total ubiquitination in the Δ*Aflvps35* mutant was much higher than that in the WT strain (Fig. S11, *D* and *E*). In conclusion, the core retromer complex cooperated with AflRab7 to control vesicle-vacuole fusion. Breaking vacuole formation caused the accumulation of ubiquitinated proteins, thereby affecting protein degradation.

Discussion

The retromer complex mediated the regulation of specific developmental and infection processes in the fungus A. flavus

The retromer complex is characterized as an important component of the endosomal protein-sorting machinery that implements the retrograde transport of cargo molecules (e.g., signaling molecules, proteins toxins) from the endosome to the Golgi apparatus or plasma membrane in various species (31, 42, 43). It has been linked to the regulation of vacuole development in *Arabidopsis* and the occurrence of neurodegenerative diseases in mammals (40, 44). Our genetic, biochemical, and morphological analyses indicate that functional disturbance in any part of the retromer subcomplex (AflVps26, AflVps29, or AflVps35) could cause severe growth and asexual reproduction defects in *A. flavus*. The regulatory effects of these three proteins in the complex have been found to be widespread throughout the fungal kingdom. In *S. cerevisiae*, Vps26 or Vps29 is essential for assisting Vps10 retrograde transportation from the vacuole to the Golgi apparatus, which is consistent with Vps35 (29). These *vps26* and *vps29* gene products also perform the same function as *vps35* in the growth, asexual reproduction development, and pathogenicity of *F. graminearum* cells (31). Knocking-out the *vps26* or *vps29* coding gene in another filamentous fungus, *M. grisea,* also had a significant effect on impaired conidiation and pathogenicity, similar to the Δ*vps35* strain. Interestingly, the retromer complex in *A. flavus* negatively controls secondary metabolic production. A phylogenic tree of Vps proteins is proposed in Fig. S12, and the result indicated that Vps26, Vps29, and Vps35 possess high conservation in their amino acid sequences in *Aspergillus* species. *A. flavus* and *Aspergillus parasiticus* share a similar toxic gene cluster and produce various aflatoxins, such as AFB1, AFB2, AFG1, and AFG2 (45). Given the findings of our study, we speculated that the retromer complex may similarly serve as a toxin regulatory protein in *A. parasiticus*. *A. fumigatus* is known to generate an important metabolite called fumagillin (46), and the fumagillin biosynthetic pathway is quite different from that in *A. flavus*. Therefore, the specific functions of the retromer complex in *A. fumigatus* need to be further explored.

Intrinsic connection among AflVps26, AflVps29, and AflVps35 plays a crucial role in the cargo-selection complex executing its core functions

The fluorescence localizations of these three Vps proteins in *A. flavus* were observed on the vacuole, which is also the prime location where the retromer complex executes its core functions in *M. grisea* or *F. graminearum* (30, 31, 42). In previous structure model (47), AflVps35 was located at the center of the trimer, AflVps26 bound the N-terminus solenoid part of AflVps35 with two β-strands of the C-terminal domain, and the N-terminal portion of AflVps29 (phosphoesterase-fold subunit) interacted with the horseshoe-shaped region of AflVps35. In the AflVps35-AflVps26 subunit, AflVps26^{E241} was associated with a highly conserved region of Vps35 (^{98}QYAGNI^{103}) for fungal orthologs, whereas peptide ^{105}PRLYL^{109} from human Vps35 is considered important for the binding of these two proteins (27, 48, 49). In this study, AflVps29 and AflVps35 shared two stable salt bridge networks, which were positioned at either end of the contact interface (Fig. 5*B*). Mutating either end of the AflVps35-interacting residues could influence the AflVps35 combining capacity of AflVps29. Human Vps35 mutants carrying one or two recognition sites even prevented assembly with Vps29 (28). In this study, AflVps35 with five residues (R865, R859, R855, R622, and R619) could block protein–protein interactions, suggesting that Vps35-Vps29 combination in *A. flavus* is more tightly controlled than that in humans. In addition, the residue Q707 on AflVps35 participated in hydrogen bond building. In non-fungal species (28), the substitution of Q707 is carried out to alanine, which offers another explanation for why AflVps35-AflVps29 possessed strong binding ability. These interactions in the AflVps26–AflVps29–AflVps35 complex are important for phenotypic characteristics, as reflected in the colonies and toxin synthesis/export of the constructed mutation strains. These results implied that the inseparable connection among AflVps26, AflVps29, and AflVps35 is essential for the core retromer complex to fully function.

Molecular mechanism by which the retromer complex regulates aflatoxin release

The dysfunction of the core retromer complex in *A. flavus* caused a pronounced increase in AFB1 production, but the increase in toxins did not originate from the transcription level of aflatoxin synthesis genes. Further studies support that Vps code-gene deletion or site-mutation strains retain high levels of toxins in their vesicles compared to the WT strain. Surprisingly, related toxin-synthesized proteins (AflD, AflM, and AflP) were also increased significantly. These results indicated that the retromer is associated with aflatoxin production but is not relevant to aflatoxin synthesis-related gene expression.

Recently, the partnership of Vps35 and Rab7 in *Arabidopsis* was found to trigger downstream events, such as the fusion of vacuoles (40). Rab7 acts as a molecular switch in the fusion of vesicles and lysosomes and is an important marker of autophagy (50–53). By microexamination, we found that the protein storage vacuoles in the Vps code-gene deletion or site-mutation strains appeared smaller than that in the WT, which differs from that observed in yeast cells (23, 24) but is similar to that in Vps35 lacking mutant strains of *Arabidopsis* (32). We speculate that the interaction of Vps35 and Rab7 is necessary for the fusion of late compartments with the vacuole in *A. flavus*. Together with other reports, we found that Rab7-

deficient strains caused incomplete growth of the vacuoles and increased aflatoxin yield in *Aspergilli* (20). In addition, ES17, a blocker of Vps35 and Rab7 binding (32), had a negative feedback on toxin release in our aflatoxin measurement. AflVps35 and AflRab7 appear to work together to control late vacuolar fusion and regulate toxin synthesis.

Retromers are typically known to assist in the retrieval of specific biomolecules from the endocytic system to the trans-Golgi transport system (21–23). Interestingly, disorders of the human retromer core complex can lead to protein traffic problems, especially several toxic proteins (tau and α-synuclein) (54, 55). For example, knockdown of the human *vps35* gene led to the accumulation of autophagosome proteins, increased levels of total protein ubiquitination, and disruption of lysosomal morphology (54, 56, 57). The ES17 molecule altered the autophagic flux and protein ubiquitination level (40). The total protein ubiquitination level in the Δ*Aflvps35* strain was much higher than that in the WT strain, indicating that the ubiquitylation of toxin-synthesized enzymes is a possible factor for the aflatoxin metabolism process.

Based on the above result, we propose a potential molecular mechanism whereby the core retromer complex regulates aflatoxin metabolism. The retromer complex is essential for vesicle-vacuole fusion in *A. flavus*. In a previous report, the blocking of vesicle-vacuole fusion acted as a checkpoint for aflatoxin production, and the abnormal upregulation of aflatoxin was related with Rab7 (20). In our study, the core retromer complex cooperated with AflRab7 to control vesicle-vacuole fusion. Destruction of vacuole formation caused the accumulation of ubiquitinated proteins, affected aflatoxin-associated protein (such as AflD, AflM, and AflP) degradation, and ultimately sped up aflatoxin synthesis.

Experimental procedure

Strains and culture conditions

A. flavus CA14 PTs (58) and all the fungal mutants constructed in this study are listed in Table S1. All strains were cultured on potato dextrose agar (PDA) medium, sclerotia-inducing Wickerham medium, and peanut medium for the study of mycelial growth, sclerotia production, and aflatoxin production, respectively (59–61).

Mutant strain construction

All primer information is provided in Table S2. In order to obtain the Vps35-deficient strain (Δ*Aflvps35*), experiments were carried out according to a previously described method (60). A homologous recombination strategy was used. The upstream and downstream of *vps35* and the screening gene *pyrG* were amplified using specific primers (see Table S2), and then overlap PCR was used for the amplification of these three fragments (60). Fungal DNA of the transformant was extracted in small doses for verification by PCR, quantitative real-time PCR, and southern blot hybridization with a KpnI using North2South Chemiluminescent Hybridization and Detection Kit (Thermo Fisher Scientific) (62). The *vps26*, *vps29,* and *rab7* deletion strains were also constructed in the same way as *vps35*.

In order to obtain the *vps35* complementation strain (Com-*Aflvps35*), a random backfilling method was used (60). The complementary fragment of *vps35* was amplified from the ORF region of *vps35* and the promoter region at the 5′ flanking region. Primers Com-*vps35-gfp*-F and Com-*vps35-gfp*-R were used to clone the complementary fragment into the vector pTRA-GFP (see Table S2). The plasmid bearing the pyrithione resistance marker was transformed into the *vps35* deletion mutant. Selected strains were then confirmed by PCR and RT-PCR. The *vps26* and *vps29* complementation strains were also constructed in the same way as *vps35*.

Point mutations in the *A. flavus* strains were constructed using a similar construction method (59). The plasmid DNA containing the *vps35* gene fragment, the selection marker gene (*pyrG*) with 8 × HA tag, and the downstream fragment of the *vps35* gene constructed by fusion PCR amplification was cloned into the pET-28a vector, and site-directed mutagenesis was used to obtain the point mutation gene. The amplified mutant overlap fragment was then transformed into the *A. flavus* CA14 strain. The construction of the mutant strains of *vps26* was the same as the above method.

Gene cloning and protein expression and purification

The *vps35* gene of *A. flavus* was amplified by PCR from the cDNA library of *A. flavus* and cloned into the pET-28a and pEGX-6P1 expression vector (Novagen). The construct contained a 6 × His-tag or GST-tag, followed by a PreScission protease cleavage site at the N-terminus of Vps35 (Vps35-N). The plasmid containing the sequenced target gene was transformed into *E. coli* BL21 (DE3) competent cells (Invitrogen). According to the aforementioned method (59–61), IPTG was used to induce the expression of the target protein. The cell pellets were resuspended in binding buffer A (50 mM Tris–HCl, 500 mM NaCl, pH 8.0) and then sonicated on ice. The fusion protein with 6 × His-tag was eluted with a gradient concentration of imidazole buffer (59), and the GST fusion protein was eluted with a gradient concentration of reduced glutathione buffer (25). The method for Vps26, Vps29, AflD, AflM, and AflP construction was the same as the above method.

Molecular modeling

The initial structures of the protein complexes Vps35-Vps29 and Vps35-Vps26 were obtained using cryo-EM (PDB ID: 6h7w) (25). Missing residues in the complexes were fixed by employing the SWISS-MODEL homology modeling server (63). All-atomic MD simulations were conducted using the GROMACS 5.1.4 package (64). Each full-length complex was solvated in 0.15 mol/l NaCl solution, resulting in a simulation unit cell with approximately 50,000 atoms. The periodic boundary condition was applied in all three dimensions. The AMBER ff99SB-ildn force field was employed to describe the protein complex (65). Water and ions were represented by the TIP3P model and the Joung-Cheatham model, respectively

(66, 67). Van der Waals interactions were truncated at 10 Å. Short-range Coulombic interactions were cut off at 10 Å, while long-range Coulombic interactions were treated with the particle mesh Ewald approach (68). The system first went through a 5000-step run of conjugated gradient minimization. A 500-ns MD simulation was then conducted in the isothermal-isobaric (NPT) ensemble at 300 K and 1 bar. Constant temperature and pressure were maintained using the Nosé-Hoover thermostat and the Parrinello-Rahman barostat, respectively (69). Note that the first 100 ns were for equilibration and the last 400 ns were for analysis. A hydrogen bond was identified to be present if (1) the distance between the acceptor atom and the donor atom was less than 3.5 Å, and (2) the angle at the hydrogen atom was greater than 150°.

Immunoblot and immunoprecipitation analysis

In order to obtain the corresponding serum antibodies, the purified AflM, AflD, AflP, Vps35 N, Vps26, Vps29, and Rab7 proteins were respectively injected into 6-week-old female BALB/c mice using the method described earlier (59–61). All serum antibodies in this study were produced by Willget Biotech Company, and the obtained serum was used as the primary antibody in Western blot verification. All animal experiments in this study followed the protocol approved by the Animal Ethics Committee of Fujian Agriculture and Forestry University. The specific steps of the total protein extraction and Western blot were described in detail in a previous article (59–61). For the extraction of the total protein in the western detection of toxin-related proteins, the mycelia cultured under the same conditions for toxin detection were used, and the protein extract was dissolved in RIPA buffer. Total protein normalized quantification was performed on SDS-PAGE gel. Western blots were subsequently performed using the corresponding primary antibodies. Visualization and semi-quantitative analysis were performed using G:BOX Chemi XT4 (Syngene).

For the immunoprecipitation of HA-fusion proteins from cellular extracts, equal concentrations of total proteins were isolated and incubated with 50 μl of anti-HA magnetic beads (MedChemExpress) following the manufacturer's instructions and then analyzed by immunoblot detection with the anti-Vps35N, anti-Vps26, anti-Rab7 (Willget Biotech Company), anti-Ubiquitin (PTM BIO), or anti-HA (Sigma-Aldrich) antibodies.

Analysis of vegetative growth and formation of conidia and sclerotia

The colony morphology and growth rate were studied using PDA medium according to a previous publication (59). The PDA medium was cultured at 37 °C in the dark for 4 days, and the diameter of the colonies was measured to study the differences in colony growth of the different strains. For the observation of mycelial morphology, the spore fluid was evenly coated on the PDA medium. The sterile coverslips were placed on the medium and cultured in the dark at 37 °C for 3 days. After the hyphae grew on the coverslips, the coverslips were taken out and placed in CFW solution. The morphology of the hyphae and the growth of the diaphragm were observed under a fluorescence microscope. For the observation and counting of the number of spores, the colony spores cultivated in the dark for 4 days in the PDA medium were washed with 2 ml sterile water, and the spore solution was diluted to a certain number and counted by a hemocytometer under a microscope. For the observation of sporozoites, PDA medium was used for culture at 37 °C for 2 days, and the surface mycelium of the colony was scraped off. The edge of the colony was cut out and placed on a cover slip and cultured in the dark at 37 °C for 12 h, and the growth and development of the conidiophore of different strains were observed under a microscope. For the observation of the number of sclerotia of different strains, Wickerham medium was cultured at 37 °C in the dark for 7 days, the hyphae were washed with 75% alcohol, and the growth of the sclerotia was observed (62).

Aflatoxin extraction and analysis

For aflatoxin analysis, the strains were cultured on peanut medium in the dark at 29 °C for 7 days. For the extraction of toxins in vesicle-vacuole fractions, we referred to (70), using the same weight of mycelial block for the extraction of vesicle-vacuole fractions and maintaining consistency in all amounts in subsequent operations. For the *in vitro* toxin quantification of *A. flavus*, the dry mycelium was weighed. The dried toxin samples of each strain were dissolved in the same dichloromethane. According to the dry weight of the mycelium, the samples were loaded on a TLC plate in the same proportion as the dry weight (59). The HPLC method referred to the aforementioned method (71), and aflatoxin was detected by an HPLC system (Water) on a MYCOTOX reversed phase C18 column.

Acquisition and processing of fluorescence images

In order to locate the Vps protein in the fungal cells, the Vps-GFP fusion protein was constructed with reference to the construction method of the above-mentioned complementary strain. Mycelia were harvested after overnight incubation in PDA medium and washed twice with PBS to wash off the medium. Fifty micromoles of FM4-64 staining solution (Bio-Dee) or 5 μM CMAC (Thermo Fisher Scientific) staining solution were applied for 30 min on ice. After three washes with PBS, the hyphae were placed on slides and the subcellular localization of the GFP-coexpressed proteins was identified using a confocal laser scanning microscope (Leica SP8). GFP was excited with a 488 nm laser; FM4-64 was excited with a 558 nm laser; and CMAC was excited with a 353 nm laser. Fluorescence emissions were measured at 507 nm, 734 nm, and 466 nm for GFP, FM4-64, and CMAC, respectively.

Chemical treatments

ES17 (Vitas-M Laboratory) was diluted in DMSO to 5 mg/ml aliquots and stored in a −20 °C freezer in the dark. Then, 250 μM of ES17 was added to 1 ml of PDA medium using a 24-well plate, and the same amount of DMSO was added as a

control. The plate was incubated in the dark at 37 °C for 2 days to observe the phenotypic inhibition and for diameter measurements. In the experiment of the effect of ES17 on aflatoxin, ES17 was added to peanut medium using a similar method and cultivated in the dark at 29 °C for 7 days. The toxins were detected as previously described.

Seed pathogenicity analysis

A previous method was followed for the detection of seed pathogenicity (59). Peanuts and maize kernels of similar size were selected and washed with sodium hypochlorite, sterile water, 75% ethanol, ethanol, and sterile water. The spore liquid (5×10^6) was soaked for 30 min and then placed in the dark at 28 °C for 5 to 6 days, following which the spore number and toxin content were tested.

Stress assays

In order to observe the response of the defective strains to different stress environments, fresh spore fluid of each strain was diluted to a concentration of 1×10^6 cells/ml. PDA medium was poured with various inhibitors into a 6-cm disposable culture dish. Oxidative stress (3 mmol/l H_2O_2 and 0.8 mmol/l tBOOH), cell wall stress (300 μg/ml Congo Red), cell membrane stress (100 μg/ml sodium lauryl sulfate) treatments, and a PDA medium control group without an additive were set. After the diluted spore solution was thoroughly mixed, 1 μl spore solution was inoculated into the center of a petri dish, and the colony diameter was measured every 24 h.

RNA isolation and real-time quantitative RT-PCR

The *A. flavus* mycelium was collected, and TRIzol (Biomarker Technologies) was used to extract the total mycelium RNA according to the method described in a previous study (60). The RNA was reverse transcribed into cDNA by using a reverse transcription kit (Thermo Fisher Scientific) (60). Specific primers were used to perform quantitative PCR with cDNA as template, and WT *A. flavus* cDNA was used as a control.

Statistical analysis

GraphPad Prism 5.0 (GraphPad Software) was used for statistical and significance analysis at a p-value less than 0.05. Statistical significance was analyzed using one-way ANOVA. All statistical tests had three biological parallels, unless specified otherwise.

Data availability

The data that support the findings of this study are available in the RCSB PDB protein data bank at [https://doi.org/10.2210/pdb6H7W/pdb], reference number (25). These data were derived from the following resources available in the public domain: [https://www1.rcsb.org/structure/6h7w].

Supporting information—This article contains supporting information (58, 72).

Acknowledgments—This work was supported by the National Natural Science Foundation of China (Grant Nos. 31972214), the Fund for Outstanding Doctoral Dissertation (Fujian Agriculture and Forestry University), and the Science and Technology Innovation Fund of Fujian Agriculture and Forestry University (CXZX2020051A). We thank LetPub (www.letpub.com) for its linguistic assistance during the preparation of this article.

Author contributions—Sen Wang, Y. W., K. Y., and X. N. conceptualization; Sen Wang, Y. L., and K. Y. investigation; Sen Wang, writing–original draft; Y. W. and Shihua Wang writing–review and editing; Y. L., M. L., W. Z., L. Q., and R. L. validation; L. L., J. L., and L. J. formal analysis; S. W. supervision; S. W. funding acquisition.

Conflict of interest—The authors declare that they have no conflicts of interest with the contents of this article.

Abbreviations—The abbreviations used are: cDNA, complementary DNA; CoIP, coimmunoprecipitation; PDA, potato dextrose agar; Rab, Ras-associated binding GTPase; Ypt, yeast protein transport.

References

1. Amaike, S., and Keller, N. P. (2011) Aspergillus flavus. *Annu. Rev. Phytopathol.* **49**, 107–133
2. Yu, J., Cleveland, T. E., Nierman, W. C., and Bennett, J. W. (2005) Aspergillus flavus genomics: gateway to human and animal health, food safety, and crop resistance to diseases. *Rev. Iberoam. Micol.* **22**, 194–202
3. Klich, M. A. (2007) Aspergillus flavus: the major producer of aflatoxin. *Mol. Plant Pathol.* **8**, 713–722
4. Hedayati, M. T., Pasqualotto, A. C., Warn, P. A., Bowyer, P., and Denning, D. W. (2007) Aspergillus flavus: human pathogen, allergen and mycotoxin producer. *Microbiology (Reading, England)* **153**, 1677–1692
5. Cardwell, K. F., and Henry, S. H. (2004) Risk of exposure to and mitigation of effect of aflatoxin on human health: a west african example. *Toxin Rev.* **23**, 213–235
6. Farombi, E. O. (2006) Review-Aflatoxin contamination of foods in developing countries: implications for hepatocellular carcinoma and chemopreventive strategies. *Acad. J.* **5**, 1–14
7. Gong, Y., Hounsa, A., Egal, S., Turner, P. C., Sutcliffe, A. E., Hall, A. J., *et al.* (2004) Postweaning exposure to aflatoxin results in impaired child growth: a longitudinal study in Benin, west africa. *Environ. Health Perspect.* **112**, 1334
8. Bennett, J. W., and Klich, M. (2009) Mycotoxins. *Encyclopedia Microbiol.* **16**, 559–565
9. Yu, J., Chang, P. K., Ehrlich, K. C., Cary, J. W., Bhatnagar, D., Cleveland, T. E., *et al.* (2004) Clustered pathway genes in aflatoxin biosynthesis. *Appl. Environ. Microbiol.* **70**, 1253
10. Brown, D. W., Kelkar, H. S., Fernandes, M., Nesbitt, T. C., Keller, N. P., Adams, T. H., *et al.* (1996) Twenty-five coregulated transcripts define a sterigmatocystin gene cluster in Aspergillus nidulans. *Proc. Natl. Acad. Sci. U. S. A.* **93**, 1418
11. Chang, P. K. (2003) The Aspergillus parasiticus protein AFLJ interacts with the aflatoxin pathway-specific regulator AFLR. *Mol. Genet. Genomics* **268**, 711–719
12. Roze, L. V., Hong, S. Y., and Linz, J. E. (2013) Aflatoxin biosynthesis: current frontiers. *Annu. Rev. Food Sci. Technol.* **4**, 293
13. Minto, R. E., and Townsend, C. A. (1997) Enzymology and molecular biology of aflatoxin biosynthesis. *Chem. Rev.* **97**, 2537–2556
14. Trail, F., Chang, P. K., Cary, J., and Linz, J. E. (1994) Structural and functional analysis of the nor-1 gene involved in the biosynthesis of aflatoxins by Aspergillus parasiticus. *Appl. Environ. Microbiol.* **60**, 4078–4085
15. Maggio-Hall, L. A., Wilson, R. A., and Keller, N. P. (2005) Fundamental contribution of beta-oxidation to polyketide mycotoxin production in planta. *Mol. Plant Microbe. Interact.* **18**, 783–793

16. Hong, S. Y., and Linz, J. E. (2009) Functional expression and sub-cellular localization of the early aflatoxin pathway enzyme Nor-1 in Aspergillus parasiticus. *Mycol. Res.* **113**, 591–601
17. Lee, L. W., Chiou, C. H., Klomparens, K. L., Cary, J. W., and Linz, J. E. (2004) Subcellular localization of aflatoxin biosynthetic enzymes Nor-1, Ver-1, and OmtA in time-dependent fractionated colonies of Aspergillus parasiticus. *Arch. Microbiol.* **181**, 204–214
18. Liang, S. H., Wu, T. S., Lee, R., Chu, F. S., and Linz, J. E. (1997) Analysis of mechanisms regulating expression of the ver-1 gene, involved in aflatoxin biosynthesis. *Appl. Environ. Microbiol.* **63**, 1058–1065
19. Hong, S. Y., and Linz, J. E. (2008) Functional expression and subcellular localization of the aflatoxin pathway enzyme Ver-1 fused to enhanced green fluorescent protein. *Appl. Environ. Microbiol.* **74**, 6385–6396
20. Chanda, A., Roze, L. V., Kang, S., Artymovich, K. A., Hicks, G. R., Raikhel, N. V., *et al.* (2009) A key role for vesicles in fungal secondary metabolism. *Proc. Natl. Acad. Sci. U. S. A.* **106**, 19533–19538
21. Seaman, M. N. J. (2012) The retromer complex – endosomal protein recycling and beyond. *J. Cell Sci.* **125**, 4693
22. Seaman, M. N. J., Marcusson, E. G., Cereghino, J. L., and Emr, S. D. (1997) Endosome to Golgi retrieval of the vacuolar protein sorting receptor, Vps10p, requires the function of the VPS29, VPS30, and VPS35 gene products. *J. Cell Biol.* **137**, 79
23. Seaman, M. N. J., Mccaffery, J. M., and Emr, S. D. (1998) A membrane coat complex essential for endosome-to-golgi retrograde transport in yeast. *J. Cell Biol.* **142**, 665
24. Nothwehr, S. F., Ha, S. A., and Bruinsma, P. (2000) Sorting of yeast membrane proteins into an endosome-to-Golgi pathway involves direct interaction of their cytosolic domains with Vps35p. *J. Cell Biol.* **151**, 297
25. Kovtun, O., Leneva, N., Bykov, Y. S., Ariotti, N., Teasdale, R. D., Schaffer, M., *et al.* (2018) Structure of the membrane-assembled retromer coat determined by cryo-electron tomography. *Nature* **561**, 561–564
26. Leneva, N., Kovtun, O., Morado, D. R., Briggs, J. A. G., and Owen, D. J. (2021) Architecture and mechanism of metazoan retromer:SNX3 tubular coat assembly. *Sci. Adv.* **7**
27. Lucas, M., Gershlick, D. C., Vidaurrazaga, A., Rojas, A. L., Bonifacino, J. S., and Hierro, A. (2016) Structural mechanism for cargo recognition by the retromer complex. *Cell* **167**, 1623–1635.e14
28. Hierro, A., Rojas, A. L., Rojas, R., Murthy, N., Effantin, G., Kajava, A. V., *et al.* (2007) Functional architecture of the retromer cargo-recognition complex. *Nature* **449**, 1063–1067
29. Iwaki, T., Hosomi, A., Tokudomi, S., Kusunoki, Y., Fujita, Y., Giga-Hama, Y., *et al.* (2006) Vacuolar protein sorting receptor in Schizosaccharomyces pombe. *Microbiology (Reading)* **152**, 1523–1532
30. Zheng, W., Zheng, H., Zhao, X., Zhang, Y., Xie, Q., Lin, X., *et al.* (2016) Retrograde trafficking from the endosome to the trans-Golgi network mediated by the retromer is required for fungal development and pathogenicity in Fusarium graminearum. *New Phytol.* **210**, 1327–1343
31. Zheng, W., Zhou, J., He, Y., Xie, Q., Chen, A., Zheng, H., *et al.* (2015) Retromer is essential for autophagy-dependent plant infection by the rice blast fungus. *PLoS Genet.* **11**, e1005704
32. Yamazaki, M., Shimada, T., Takahashi, H., Tamura, K., Kondo, M., Nishimura, M., *et al.* (2008) Arabidopsis VPS35, a retromer component, is required for vacuolar protein sorting and involved in plant growth and leaf senescence. *Plant Cell Physiol.* **49**, 142–156
33. Schmitt, H. D., Wagner, P., Pfaff, E., and Gallwitz, D. (1986) The ras-related YPT1 gene product in yeast: a GTP-binding protein that might be involved in microtubule organization. *Cell* **47**, 401–412
34. Zelazny, E., Santambrogio, M., Pourcher, M., Chambrier, P., Berne-Dedieu, A., Fobis-Loisy, I., *et al.* (2013) Mechanisms governing the endosomal membrane recruitment of the core retromer in Arabidopsis. *J. Biol. Chem.* **288**, 8815–8825
35. Rojas, R., van Vlijmen, T., Mardones, G. A., Prabhu, Y., Rojas, A. L., Mohammed, S., *et al.* (2008) Regulation of retromer recruitment to endosomes by sequential action of Rab5 and Rab7. *J. Cell Biol.* **183**, 513–526
36. Ohsumi, K., Arioka, M., Nakajima, H., and Kitamoto, K. (2002) Cloning and characterization of a gene (avaA) from Aspergillus nidulans encoding a small GTPase involved in vacuolar biogenesis. *Gene* **291**, 77–84
37. Pinar, M., and Peñalva, M. A. (2021) The fungal RABOME: RAB GTPases acting in the endocytic and exocytic pathways of Aspergillus nidulans (with excursions to other filamentous fungi). *Mol. Microbiol.* **116**, 53–70
38. Nakada-Tsukui, K., Saito-Nakano, Y., Ali, V., and Nozaki, T. (2005) A retromerlike complex is a novel Rab7 effector that is involved in the transport of the virulence factor cysteine protease in the enteric protozoan parasite Entamoeba histolytica. *Mol. Biol. Cell* **16**, 5294–5303
39. Priya, A., Kalaidzidis, I. V., Kalaidzidis, Y., Lambright, D., and Datta, S. (2015) Molecular insights into rab7-mediated endosomal recruitment of core retromer: deciphering the role of Vps26 and Vps35. *Traffic* **16**, 68–84
40. Rodriguez-Furlan, C., Domozych, D., Qian, W., Enquist, P. A., Li, X., Zhang, C., *et al.* (2019) Interaction between VPS35 and RABG3f is necessary as a checkpoint to control fusion of late compartments with the vacuole. *Proc. Natl. Acad. Sci. U. S. A.* **116**, 21291–21301
41. Abenza, J. F., Galindo, A., Pinar, M., Pantazopoulou, A., de los Ríos, V., and Peñalva, M. A. (2012) Endosomal maturation by Rab conversion in Aspergillus nidulans is coupled to dynein-mediated basipetal movement. *Mol. Biol. Cell* **23**, 1889–1901
42. Xie, Q., Chen, A., Zheng, W., Xu, H., Shang, W., Zheng, H., *et al.* (2016) ESCRT-0 complex is required for fungal development and pathogenicity in Fusarium graminearum. *Environ. Microbiol.* **18**, 3742–3757
43. Mitsui, K., Koshimura, Y., Yoshikawa, Y., Matsushita, M., and Kanazawa, H. (2011) The endosomal Na+/H+ exchanger contributes to multivesicular body formation by regulating the recruitment of ESCRT-0 Vps27p to the endosomal membrane. *J. Biol. Chem.* **286**, 37625–37638
44. Trousdale, C., and Kim, K. (2015) Retromer: structure, function, and roles in mammalian disease. *Eur. J. Cell Biol.* **94**, 513–521
45. Smith, M. C., Madec, S., Coton, E., and Hymery, N. (2016) Natural Co-occurrence of mycotoxins in foods and feeds and their *in vitro* combined toxicological effects. *Toxins (Basel)* **8**, 94
46. Guruceaga, X., Perez-Cuesta, U., Abad-Diaz de Cerio, A., Gonzalez, O., Alonso, R. M., Hernando, F. L., *et al.* (2019) Fumagillin, a mycotoxin of Aspergillus fumigatus: biosynthesis, biological activities, detection, and applications. *Toxins (Basel)* **12**, 7
47. Harbour, M. E., and Seaman, M. N. J. (2011) Evolutionary variations of VPS29, and their implications for the heteropentameric model of retromer. *Commun. Integr. Biol.* **4**, 619
48. Zhao, X., Nothwehr, S., Lara-Lemus, R., Zhang, B.-Y., Peter, H., and Arvan, P. (2008) Dominant-negative behavior of mammalian Vps35 in yeast requires a conserved PRLYL motif involved in retromer assembly. *Traffic (Copenhagen, Denmark)* **8**, 1829–1840
49. Gokool, S., Tattersall, D., Reddy, J., and Seaman, M. (2008) Identification of a conserved motif required for Vps35/Vps26p interaction and assembly of the retromer complex. *Biochem. J.* **408**, 287–295
50. Liu, J., Lei, M., Zhou, Y., and Chen, F. (2019) A comprehensive analysis of the small GTPases Ypt7 involved in the regulation of fungal development and secondary metabolism in monascus ruber M7. *Front. Microbiol.* **10**, 452
51. Kashiwazaki, J., Nakamura, T., Iwaki, T., Takegawa, K., and Shimoda, C. (2005) A role for fission yeast Rab GTPase Ypt7p in sporulation. *Cell Struct. Funct.* **30**, 43–49
52. Li, Y., Li, B., Liu, L., Chen, H., Zhang, H., Zheng, X., *et al.* (2015) FgMon1, a guanine nucleotide exchange factor of FgRab7, is important for vacuole fusion, autophagy and plant infection in Fusarium graminearum. *Sci. Rep.* **5**, 18101
53. Wen, H., Zhan, L., Chen, S., Long, L., and Xu, E. (2017) Rab7 may be a novel therapeutic target for neurologic diseases as a key regulator in autophagy. *J. Neurosci. Res.* **95**, 1993–2004
54. Carosi, J. M., Hein, L. K., van den Hurk, M., Adams, R., Milky, B., Singh, S., *et al.* (2021) Retromer regulates the lysosomal clearance of MAPT/tau. *Autophagy* **17**, 2217–2237
55. Tang, F. L., Erion, J. R., Tian, Y., Liu, W., Yin, D. M., Ye, J., *et al.* (2015) VPS35 in dopamine neurons is required for endosome-to-golgi retrieval of Lamp2a, a receptor of chaperone-mediated autophagy that is critical for α-synuclein degradation and prevention of pathogenesis of Parkinson's disease. *J. Neurosci.* **35**, 10613–10628

56. Tang, F. L., Zhao, L., Zhao, Y., Sun, D., Zhu, X. J., Mei, L., *et al.* (2020) Coupling of terminal differentiation deficit with neurodegenerative pathology in Vps35-deficient pyramidal neurons. *Cell Death Differ.* **27**, 2099–2116
57. Filippone, A., Li, J. G., and Praticò, D. (2021) VPS35 downregulation alters degradation pathways in neuronal cells. *J. Alzheimer's Dis.* **84**, 1079–1089
58. Chang, P. K., Scharfenstein, L. L., Wei, Q., and Bhatnagar, D. (2010) Development and refinement of a high-efficiency gene-targeting system for Aspergillus flavus. *J. Microbiol. Methods* **81**, 240–246
59. Wang, Y., Wang, S., Nie, X., Yang, K., Xu, P., Wang, X., *et al.* (2019) Molecular and structural basis of nucleoside diphosphate kinase–mediated regulation of spore and sclerotia development in the fungus Aspergillus flavus. *J. Biol. Chem.* **294**, 12415–12431
60. Yang, K., Liu, Y., Wang, S., Wu, L., Xie, R., Lan, H., *et al.* (2019) Cyclase-associated protein cap with multiple domains contributes to mycotoxin biosynthesis and fungal virulence in Aspergillus flavus. *J. Agric. Food Chem.* **67**, 4200–4213
61. Yang, G., Yue, Y., Ren, S., Yang, M., Zhang, Y., Cao, X., *et al.* (2019) Lysine acetylation contributes to development, aflatoxin biosynthesis and pathogenicity in Aspergillus flavus. *Environ. Microbiol.* **21**, 4792–4807
62. Zhang, F., Geng, L., Deng, J., Huang, L., Zhong, H., Xin, S., *et al.* (2020) The MAP kinase AflSlt2 modulates aflatoxin biosynthesis and peanut infection in the fungus Aspergillus flavus. *Int. J. Food Microbiol.* **322**, 108576
63. Andrew, W., Martino, B., Stefan, B., Gabriel, S., Gerardo, T., Rafal, G., *et al.* (2018) SWISS-MODEL: homology modelling of protein structures and complexes. *Nucl. Acids Res.* **46**, W296–W303
64. Abraham, M., Murtola, T., Schulz, R., Páll, S., Smith, J., Hess, B., *et al.* (2015) GROMACS: high performance molecular simulations through multi-level parallelism from laptops to supercomputers. *SoftwareX* **1**, 19–25
65. Lindorff-Larsen, K., Piana, S., Palmo, K., Maragakis, P., Klepeis, J. L., Dror, R. O., *et al.* (2010) Improved side-chain torsion potentials for the Amber ff99SB protein force field. *Proteins* **78**, 1950–1958
66. Jorgensen, W., Chandrasekhar, J., Madura, J., Impey, R., and Klein, M. (1983) Comparison of simple potential functions for simulating liquid water. *J. Chem. Phys.* **79**, 926–935
67. Joung, I., and Cheatham, T. (2008) Determination of alkali and halide monovalent ion parameters for use in explicitly solvated biomolecular simulations. *J. Phys. Chem. B* **112**, 9020–9041
68. Darden, T., York, D., and Pedersen, L. (1993) Particle mesh Ewald: an N·log(N) method for Ewald sums in large systems. *J. Chem. Phys.* **98**, 10089–10092
69. Parrinello, M. R. A., and Rahman, A. J. (1982) Polymorphic transitions in single crystals: a new molecular dynamics method. *J. Appl. Phys.* **52**, 7182–7190
70. Yang, M., Zhu, Z., Bai, Y., Zhuang, Z., Ge, F., Li, M., *et al.* (2021) A novel phosphoinositide kinase Fab1 regulates biosynthesis of pathogenic aflatoxin in Aspergillus flavus. *Virulence* **12**, 96–113
71. Li, D., Qin, L., Wang, Y., Xie, Q., Li, N., Wang, S., *et al.* (2019) AflSte20 regulates morphogenesis, stress response, and aflatoxin biosynthesis of Aspergillus flavus. *Toxins (Basel)* **11**
72. Caceres, I., Khoury, A. A., Khoury, R. E., Lorber, S., Oswald, I. P., Khoury, A. E., *et al.* (2020) Aflatoxin biosynthesis and genetic regulation: a Review. *Toxins (Basel)* **12**